JOURNAL OF MATERIALS SCIENCE 12 (1977) 1143–1160

Surface re-equilibration kinetics of nonstoichiometric oxides

JANUSZ NOWOTNY
Research Laboratories of Catalysis and Surface Chemistry, Polish Academy of Sciences, ul. Niezapominajek, 30–239 Kraków, Poland

The sorption of small oxygen doses on initially equilibrated oxide surfaces is accompanied by changes in the work function with time, involving initial charging (due to chemical sorption of oxygen), passing through a maximum, and a final discharging. The final discharging is assumed to be rate controlled by chemical diffusion through the oxide surface layer. The kinetics of the changes in work function accompanying the re-equilibration process were measured for NiO, lithium-doped NiO (0.13 at. % Li_2O) CoO, and Co_3O_4. The rate constants of the discharging processes were determined as a function of temperature giving the following activation energy values, respectively: 29 kcal mol^{-1} (300 to 425° C), 1 kcal mol^{-1} (200 to 300° C); 17.8 kcal mol^{-1} (300 to 400° C); 18.3 kcal mol^{-1} (175 to 350° C); 19.9 kcal mol^{-1} (225 to 350° C).

The kinetics of sorption of oxygen were measured for undoped NiO in the temperature range 200 to 400° C, giving a change in activation energy at 300° C from 33.9 kcal mol^{-1} above, and 11 kcal mol^{-1} below the temperature. It was concluded that above 300° C the NiO lattice becomes sufficiently mobile to enable ionic transport to take place. This temperature corresponds well to the temperature at which several other properties of NiO also change.

The work function data obtained for an $NiO–Li_2O$ solid solution suggest a different mechanism of lithium incorporation into the bulk and the surface layer of NiO. The kinetic data for both CoO and Co_3O_4 indicate that the chemical diffusivity of the boundary layer of these oxides does not depend on the structure of the crystalline bulk.

The presented results indicate that the work function method is suitable for studying the transport properties of the boundary layer of non-stoichiometric oxides.

1. Introduction

The re-equilibration process in non-stoichiometric oxides involves the propagation of a chemical gradient through the crystal when the initially equilibrated oxide tends to reach its new equilibrium state. The re-equilibration kinetics provide information about the motion of lattice ions in the concentration gradient (chemical diffusivity) and can be followed by measuring the changes of any parameter reflecting the change of non-stoichiometry. The determination of the chemical diffusion coefficient in non-stoichiometric oxides, using the measurements of a physical property which is a function of the deviation from the stoichiometric composition, e.g. electrical conductivity or weight change, has been widely described by Wagner and co-workers [1–4].

Equilibration kinetic data are generally considered to be related to the bulk of the crystalline grain. It has been stated, however, that the crystal surface layer may differ essentially from the bulk in defect structure [5–8], composition [9, 10] and even crystalline structure [11]. Thus the crystalline grain of the oxide may be considered as an "heterophase system" composed of the

regular structure of the bulk and of the surface layer. Thus the problem of pertinent interpretation of the equilibration kinetic data arises, i.e. whether they are to be correlated to the crystalline bulk or to the surface layer. Moreover, if the kinetics of equilibration between the bulk of the oxide crystal and oxygen partial pressure in the ambient gas phase are rate controlled by the surface layer, then the knowledge of the transport properties of this layer seems to be of essential importance in the understanding and correct interpretation of the mechanism of such processes as oxidation of metals, reduction of ores, preparation of metal oxides, solid state reactions and certain phenomena of semiconductors.

Considering the heterophase system oxygen–non-stoichiometric oxide, the partial equilibria of both oxygen chemisorption and its incorporation into the lattice should be taken into account. Shifts of these equilibria are accompanied by electronic transitions represented quantitatively by changes in the Fermi level position, which may be directly measured by the work function technique [12–14].

Measurements of the work function have been widely appreciated by workers studying metallic surfaces [15–21]. Metals are particularly convenient for surface studies because they are relatively easily outgassed and cleaned of adsorbed impurities, thus leading to reproducible results. The interaction of oxygen with the surface of metallic films has been extensively studied by Delchar and Tompkins [16], Roberts and Wells [21, 23, 24], Shurmovskaya and Burshtein [25], Huber and Kirk [19, 20] and Dus [22]. These works illustrate well the initial steps of oxygen–metal interaction involving a metal undergoing surface corrosion. On the other hand, the surface of metal oxides is a very inconvenient object for investigation, because it is very difficult to outgass and thus to be well defined. Consequently, the reproducibility of the work function data for metal oxides requires suitable and careful standardization of the samples [26]. Application of the work function measurements in studying metal oxides has been mainly directed towards the investigation of the electronic effect accompanying chemisorption, and modification of metal oxide structure by the formation of solid solutions, in order to obtain information about the role of the electronic factor in chemisorption and catalysis on semiconducting oxide materials [6–8, 11, 27–31].

The purpose of the present work is to study the surface re-equilibration kinetics of several non-stoichiometric oxides using the work function technique. The work function measurements were used here to follow changes in surface charge generated by a concentration gradient of oxygen which was imposed on the initially equilibrated oxide surface by covering the surface with an appropriate number of oxygen atoms (oxygen dose), as described previously [32, 33]. In this case, the re-equilibration is accompanied by two electrical effects of opposite signs which take place simultaneously, but appear with different rates. These effects involve: (1) charging the surface by ionization of the adsorbed oxygen species and generation of a concentration gradient of electron carriers in the boundary layer, and (2) discharging the surface by incorporation of the oxygen into the oxide lattice until a new equilibrium state is achieved. The superimposition of these effects produces complex characteristics of the work function changes versus time curve exhibiting an extremum. Using the kinetic equation for the work function changes versus time proposed previously [32] the kinetic data referring to (1) oxygen chemisorption and (2) transport properties of the oxide surface layer may be determined. The kinetics of oxygen sorption will also be examined.

In the present investigation, polycrystalline samples of several oxide materials (NiO, lithium-doped NiO, CoO and Co_3O_4) were used. Both undoped and lithium-doped NiO as well as CoO are relatively well known and thus can be used conveniently for the surface studies as model metal-deficient oxides of the general formula $Me_{1-y}O$. There is a lack of data concerning the transport properties of the Co_3O_4 phase; however, a comparison of the surface properties of CoO and Co_3O_4 seems to be very interesting. The kinetic data of the work function changes obtained will be discussed in terms of the defect structure and transport properties of the surface layer of the oxide materials under investigation.

2. Formulation of problems and definition of terms

Assuming that an ionic oxide surface and adsorbed oxygen species create a certain capacity (a ca-

pacitor model), the following expressions have been proposed for describing the charging (Equation 1) and discharging (Equation 2) of the oxide surface:

$$\frac{d\Phi_I(t)}{dt} = \{k_I [\Delta\Phi_{max} - \Phi_I(t)]\}_{T,N_O/S=const} \quad (1)$$

$$\frac{d\Phi_D(t)}{dt} = \{k_D[\Phi_I(t) - \Phi_D(t) + \Delta\Phi_S]\}_{T,N_O/S=const}, \quad (2)$$

where $\Phi_I(t)$ = the work function changes on charging the oxide surface, produced by the ionization of the adsorbed oxygen species, after time t;

k_I = the rate constant of the charging process;

$\Delta\Phi_{max}$ = constant value related to the theoretical potential barrier corresponding to the chemisorption equilibrium;

$\Phi_D(t)$ = the work function changes on discharging the oxide surface, produced by diffusion of lattice ions;

k_D = the rate constant of the discharging process;

$\Delta\Phi_S$ = the final work function value with respect to the initial value;

T = the absolute temperature;

N_O = the number of oxygen atoms in the experimental dose;

S = the surface area of the oxide sample investigated.

The work function changes measured experimentally are the sum of $\Phi_I(t)$ and $\Phi_D(t)$ which exhibit opposite signs.

$$[\Phi_I(t) - \Phi_D(t)] = \Delta\Phi(t) \quad (3)$$

and assuming that initially:

$$\Delta\Phi(t) = 0 \text{ and } \Phi_I(t) = 0 \text{ for } t = 0, \quad (4)$$

we obtain the final form of the kinetic equation for the experimental work function changes:

$$\Delta\Phi(t) = \left\{ \frac{k_I}{k_D - k_I} \Delta\Phi_{max} [\exp(-k_I t) - \exp(-k_D t)] + \Delta\Phi_S [1 - \exp(-k_D t)] \right\}_{T,N_O/S=const} \quad (5)$$

The parameters k_I, k_D, $\Delta\Phi_{max}$ and $\Delta\Phi_S$ are related to a given oxide preparation at constant T and constant N_O/S.

According to the above assumptions, the parameters of Equation 5 should reflect some physicochemical properties of the oxide investigated. It seems appropriate to discuss these parameters and consider their relation to the surface processes occcurring during equilibration of the oxide surface. As an object for this discussion, the experimental data $\Phi(t)$ for undoped NiO will be taken for various N_O/S ratios. This is the first problem which will be considered below.

It has also been assumed that the changes in the work function in discharging the oxide surface are rate controlled by the ionic diffusion in the boundary layer [33]. Such a diffusion process taking place under a concentration gradient of defects is termed chemical diffusion [2]. Thus assuming the correlation between the rate constant k_D in Equation 5 and the chemical diffusion coefficient, one may expect that by measuring temperature dependence of the rate constant k_D one may determine the activation energy of the chemical diffusion in the oxide boundary layer. It seems suitable and interesting to compare such calculated activation energies with the activation energy of chemical diffusion determined using other methods at higher temperatures [1] as well as with the activation energy of the sorption of oxygen.

The effect of addition of lithium on the physicochemical properties of NiO has been studied extensively [6, 7, 12–14, 34–36]. Different mechanisms of lithium incorporation have been proposed for the crystalline bulk and for the surface layer [6]. There is general agreement concerning the substitutional mechanism in the bulk, but the surface mechanism is still the subject of much discussion. One would expect that the surface equilibration data may provide some information concerning the defect structure of the boundary layer of $NiO-Li_2O$ solid solutions.

CoO characteristically has a considerably larger concentration of cation vacancies than NiO, thus comparison of the surface properties of these oxides seems suitable. For the spinel structure of Co_3O_4, we expect a different diffusivity than for the rock-salt type structure of either NiO or CoO.

In considering the transport processes accompanying the charging and discharging of the surface of the metal-deficient oxides mentioned

TABLE I Spectral analysis of the preparations

No.	Impurity	Concentration (at.%)			
		Pure NiO	Lithium-doped NiO	CoO	Co_3O_4
1	nickel		–	0.01	0.05
2	cobalt	0.05	0.2	–	–
3	aluminium	0.001	0.001	ND*	0.001
4	magnesium	0.001	0.0005	< 0.0005	< 0.0005
5	manganese	0.0005	0.001	0.001	< 0.0005
6	boron	0.001	0.001	ND	ND
7	iron	< 0.0005	< 0.0005	ND	ND
8	silicon	0.001	0.001	0.001	0.0005
9	copper	0.0005	0.0005	0.001	0.001
10	zinc		0.01	ND	ND
11	lead	0.001	0.001	< 0.0005	0.0005
12	calcium	0.0005	0.0005	0.001	0.001
	Bi, Cd, Sn, Ti, Cr, V, W, Ge, Mo, Na, Ag, Au, P and Zr not detected				

*ND not detected.

above, we assume that metal ions and electron holes are the only mobile species, and the oxygen sublattice remains relatively immobile. This assumption is based on the available diffusivity data, showing that the anion sublattice of such oxides as NiO and CoO exhibits virtually no defects, and only cation vacancies may be considered as participating in the ionic transport [37]. There is a lack of diffusivity data for the Co_3O_4 phase, but transport through the cation sublattice should also be predominant here, as in other spinel structures [14]. These assumptions are valid for the crystalline bulk. We should realize, however, that due to the essential differences between the bulk and the surface layer, different transport mechanism through the layer should be expected.

3. Experimental details

3.1. Preparation of specimens

Polycrystalline preparations of NiO and CoO were obtained by calcination of basic nickel and cobalt carbonate, respectively, at 1000° C for 4 h. Co_3O_4 was obtained by decomposition of cobalt carbonate at 850° C in air for 10 h, and lithium-doped nickel oxide was prepared by evaporation to dryness of a mixture of lithium and nickel carbonate in a platinum dish, the mixture heated to 400° C for 2 h and then to 1000° C for 4 h. The excess lithium not incorporated was washed out in hot water and the mixture was then refired for 1 h at 1000° C. The final concentration of lithium was 0.13 at.%. Details of the preparation procedure are described by Bielański *et al.* [38].

The specific surface area, excess oxygen concentration detected iodometrically, and the results of spectral analysis of the preparations, are shown in Tables I and II.

3.2. Apparatus

The apparatus, including the adsorption system and the dynamic condenser for the work function measurements [39] is shown schematically in Fig. 1. The vacuum line is comprised of oil rotation and diffusion pumps (1) and (2), sorption pumps (5), low (6) and high (7) vacuum chambers, and liquid nitrogen traps (3). For chemisorption measurements, the volume of the measuring chamber can be regulated for adjusting to the most sensitive range of Pirani gauge (13) by connecting this volume with previously evacuated bulbs (8). The calibration system consists of two calibrated gas buretts (15). Oxygen is taken from one of three storage bulbs (11) which kept at different pressures depending on the oxygen dose required for the experiment. Oxygen is obtained by thermal decomposition of high purity $KMnO_4$ (12). The calibration system, as well as the calibrated bulbs

TABLE II Specific surface area and the concentration of excess oxygen of the preparations

No.	Preparation	Specific surface area ($m^2\ g^{-1}$)	Concentration of excess oxygen (at.%)
1	pure NiO	0.42	not detected
2	Li-doped NiO (0.13 at.% Li_2O)	0.502	0.03
3	CoO	0.41	0.135
4	Co_3O_4	0.81	33.3

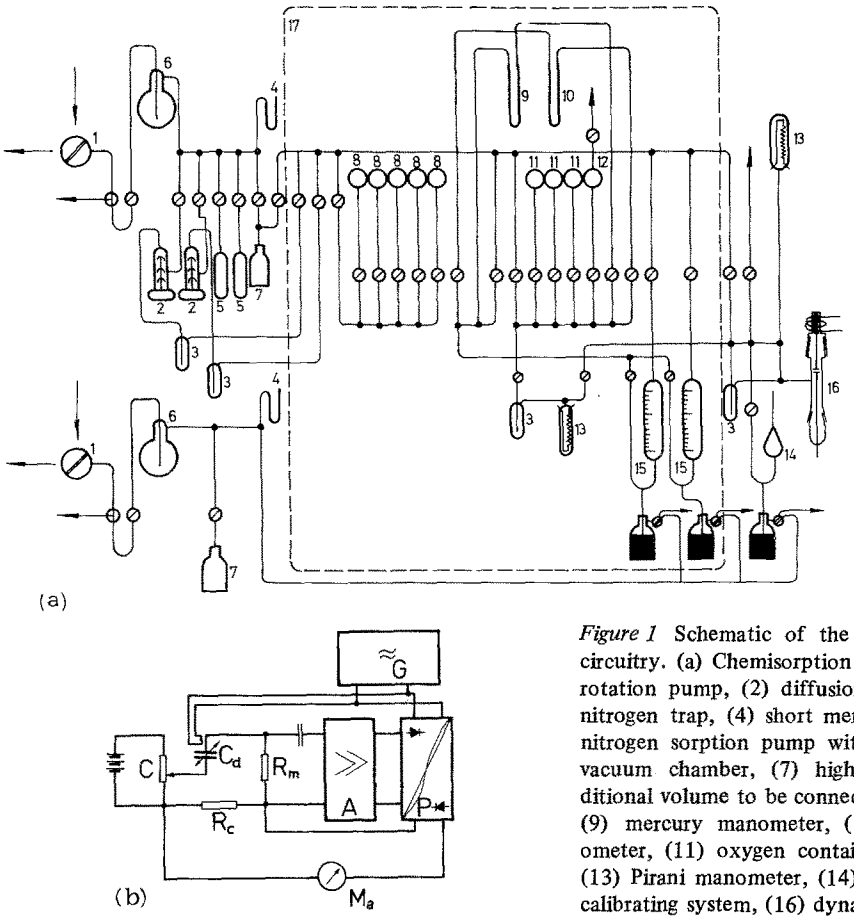

Figure 1 Schematic of the illustrations apparatus and circuitry. (a) Chemisorption and vacuum system. (1) oil rotation pump, (2) diffusion mercury pump, (3) liquid nitrogen trap, (4) short mercury manometer, (5) liquid nitrogen sorption pump with molecular sieves, (6) low vacuum chamber, (7) high vacuum chamber, (8) additional volume to be connected to the reaction chamber, (9) mercury manometer, (10) dibuthylphthalate manometer, (11) oxygen container, (12) oxygen generator, (13) Pirani manometer, (14) MacLeod manometer, (15) calibrating system, (16) dynamic condenser, (17) thermostat. (b) Electrical circuit for automatic measurements of rapid work function changes. (C) compensator, (C_d) dynamic condenser, (R_m) resistor, (G) generator, (A) amplifier, (P) phase sensitive rectifier, (Ma) ammeter, (R_c) compensation resistor.

and the measuring device, are thermostatically controlled at 25° C (17).

The dynamic condenser was used for the work function measurements [39]. It consists of two plates, the upper vibrating electrode made from platinum and the lower stainless steel electrode covered with the oxide sample to be investigated. A special electronic device made it possible to compensate automatically for the rapid changes of work function with time. The electric circuit for the measurements is shown in Fig. 1b. The dynamic condenser method consists in measuring the a.c. voltage on the resistor R_m which joins two plates of the condenser C_d when the capacitance between them varies sinusoidally. This a.c. voltage, $V_{a.c.}$, is proportional to the contact potential difference, CPD, existing between the plates:

$$V_{a.c.} = -V_{CPD}\omega R_m C_o \sin \omega t$$

where ω is frequency of the vibrations (about 60 cps) and the CPD is equal to the difference of the work function of the plates of the dynamic condenser:

$$V_{CPD} = \Phi_2 - \Phi_1 .$$

The a.c. voltage developed across the resistor R_m is fed into an amplifier, A, which is of a low-noise design. The amplified signal is then rectified in a phase-sensitive rectifier, P, which also extracts the required information from the nosiy signal by correlating it with the reference voltage of the generator, G. The d.c. output from the phase-sensitive rectifier is fed back in series with and in opposition to the CPD. Thus for the measuring circuit one can write following relationship:

$$V_{d.c.} = (V_{CPD} - V_{d.c.})\alpha$$

where $V_{d.c.}$ is a d.c. voltage drop across the compensation resistor, R_c, and α is the open loop gain. If the parameter α is sufficiently large, one may practically assume that:

$$V_{CPD} = V_{d.c.}\left(1+\frac{1}{\alpha}\right) \simeq V_{d.c.} \quad \text{for } \alpha \to \infty.$$

Thus, measurements of the changes in CPD with time consist in following the d.c. current in the output circuit of the phase-sensitive rectifier:

$$\Delta V_{CPD} \simeq \Delta V_{d.c.} = \Delta I_{d.c.} \cdot R_c.$$

When small CPD changes are to be measured, the initial value of V_{CPD} is compensated with a compensator, C. Assuming the work function changes ($\Delta\Phi_1$) of one of the plates of the dynamic condenser (platinum standardized in oxygen [31]) to be negligible under these experimental conditions, the measured value of the work function changes of the oxide sample investigated ($\Delta\Phi_2$) is thus equal to the changes of the CPD:

$$\Delta\Phi_2 \simeq \Delta V_{CPD}.$$

3.3. Experimental procedure

The amount of polycrystalline oxide samples used for each experiment was always adjusted to give a surface area equal to 0.13 m^2. The sample was spread onto the lower electrode forming a layer about 0.5 mm thick.

The sample to be investigated was previously standardized by heating under 10 mm Hg oxygen pressure at 400° C for 1 h and then outgassed at 10^{-6} mm Hg for 1 h at this temperature. Measurements were made on the samples after adjusting the temperature to the desired level.

Measurements were preceded by introduction of oxygen into the dynamic condenser according to the following procedure. An appropriate oxygen dose, accurately known, was first admitted into the small space between two stopcocks. This space, with the oxygen containers on one side and the reaction chambers on the other, was connected with the Pirani manometer and a liquid nitrogen trap. The stopcock connecting this volume with the chamber of the dynamic condenser was then opened, and pressure and work function changes registered from this moment at given intervals of time. The initial oxygen pressures in the reaction chamber were determined in the same way with no sample in the dynamic condenser. During this calibration procedure the oxygen pressure reached a constant value within about 30 sec. Table III shows the different oxygen doses used in the experiments (denoted as A_1, A_2, A_3, A_4, A_5 and A_∞) as well as the corresponding initial oxygen pressures and equivalent fractions of the monolayer coverage. These fractions were calculated assuming the number of active adsorption sites for both NiO and CoO to be equal to the number of surface cations (1.1×10^{19} m^{-2} [40].

4. Results

4.1. Undoped NiO

NiO samples which had been standardized and outgassed under 10^{-6} mm Hg, were subjected to increasing doses of oxygen (indicated in Table III as A_1, A_2, A_3, A_4 and A_∞). As seen from Fig. 2a, the increasing oxygen dose produces a marked change in the shape of experimental curves A_1 to A_4, which show all an initial increase, but then decrease after an increasing delay in appearance of the $\Delta\Phi(t)$ maximum, whereas curve A_∞ reaches a maximum and then remains constant. It can also be seen that the falling part of the curves becomes steeper with decreasing oxygen dose.

The $\Delta\Phi(t)$ runs for oxygen doses A_1 to A_4 were accompanied by a rapid decrease in oxygen pressure reaching about 10^{-5} mm Hg at the time

TABLE III Experimental oxygen doses expressed in moles and in equivalent % monolayer coverage, and corresponding initial pressures in the measuring chamber

No.	Notation	Oxygen dose		Corresponding initial oxygen pressure (mm Hg)
		moles ($\times 10^7$)	eq. % monolayer coverage	
1	A_1	0.423	4.1	9.2×10^{-4}
2	A_2	1.24	12.0	2.7×10^{-3}
3	A_3	2.53	24.1	5.5×10^{-3}
4	A_4	3.68	35.7	8.0×10^{-3}
5	A_5	3.6	34.0	7.7×10^{-3}
6	A_∞	4.52	42.7×10^3	10.0

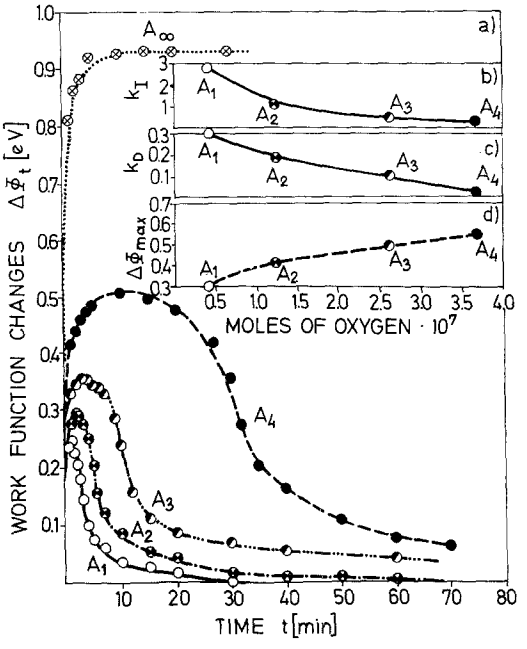

Figure 2 (a) Work function changes for NiO versus time for various oxygen doses (A_1, A_2, A_3, A_4) and for constant oxygen pressure (10 mm Hg, A_∞) at 400° C; (b) k_I versus oxygen dose, (c) k_D versus oxygen dose, (d) $\Delta\Phi_{max}$ versus oxygen dose.

corresponding to the appearance of the maximum $\Delta\Phi(t)$. This indicates that practically the whole oxygen dose is always consumed by sample. Fig. 3 illustrates the fractions of oxygen consumed by an NiO sample as a function of time, for doses A_1 to A_4. The oxygen consumption was measured from changes in oxygen pressure over the sample. The parameters k_I, k_D, $\Delta\Phi_{max}$ and $\Delta\Phi_S$ of Equation 5 were calculated for runs A_1 to A_4. These parameters are plotted versus the oxygen dose in Fig. 2b to d. It is noted that both k_I and k_D decrease, whereas $\Delta\Phi_{max}$ increases with increasing oxygen dose. $\Delta\Phi_S$ is equal to 0.05 and 0.03 eV for runs A_4 and A_3, respectively, whereas it is equal to zero for both A_1 and A_2.

Further experiments were performed by measuring the changes in work function as a function of time at various temperatures, in order to determine the activation energy of the rate controlling process for discharging the surface. These experiments were performed over the temperature range 175 to 425° C for dose A_1 (Fig. 4), and over 325 to 425° C for oxygen doses A_2 and A_3. Except for the curve for the lowest temperature, 175° C, all curves exhibited a more or less pronounced maxima. The falling part of these curves becomes steeper as the temperature increases. The nature of the $\Delta\Phi(t)$ versus time curves for doses A_2 and A_3 was analogous to that obtained for dose A_1.

Table IV shows the parameters of Equation 5 calculated for the smallest oxygen dose, A_1. The parameter k_D fits the Arrhenius-type relationship, illustrated in Fig. 5, well. The plot of log k_D versus $1/T$ can be divided into two linear parts which intersect each other at 300° C exhibiting high- and low-activation energy ranges (curves 1 and 1a, respectively). The values of log k_D obtained for larger oxygen doses, A_2 and A_3, were also plotted in Fig. 5 (curves 2 and 3, respectively) showing an activation energy of ~ 29 kcal mol^{-1} 1, the same as for dose A_1, above 300° C. The activation energy determined below 300° C for dose A_1 is equal to 1.0 kcal mol^{-1}. A least squares analysis yielded the

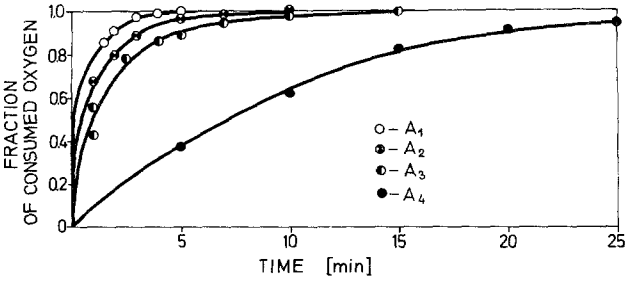

Figure 3 Fraction of consumed oxygen for undoped NiO versus time for different doses of oxygen at 400° C (corresponding to the work function changes illustrated in Fig. 2a).

TABLE IV Parameters of Equation 5 for undoped NiO (oxygen dose A_1)

	Temperature (°C)										
	175	200	225	250	275	300	325	350	375	400	425
k_I(min^{-1})	0.78	0.80	0.84	0.92	1.00	1.12	1.28	2.16	2.64	2.88	10.22
k_D(min^{-1})	0.006	0.0065	0.0075	0.0076	0.0077	0.008	0.034	0.06	0.163	0.31	0.96
$\Delta\Phi_{max}$(eV)	0.08	0.110	0.120	0.150	0.180	0.240	0.280	0.280	0.320	0.310	0.250
$\Delta\Phi_S$(eV)	0	0	0	0	0	0	0	0	0	0	0

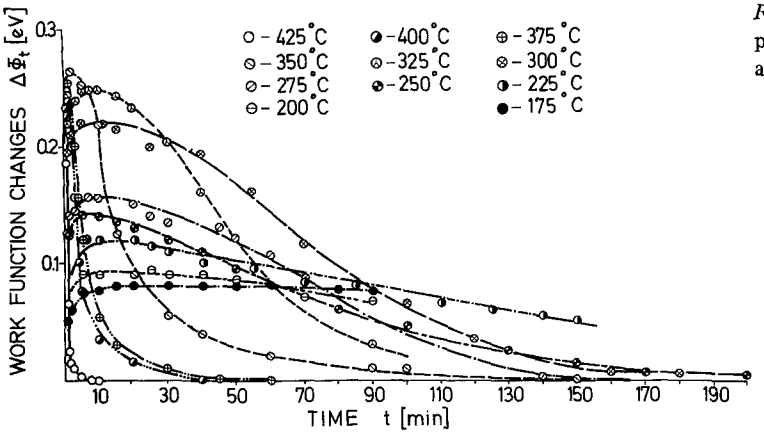

Figure 4 Work function changes $\Delta\Phi$ plotted versus time for undoped NiO and the smallest oxygen dose, A_1.

following relationships for the rate constant k_D versus temperature:

$$k^1_{D(NiO)} = \left[0.969 \times 10^9 \exp\left(-\frac{28900 \pm 1600}{RT}\right)\right]_{A_1,\ 573\,K < T < 698\,K} \tag{6}$$

$$k^2_{D(NiO)} = \left[0.705 \times 10^9 \exp\left(-\frac{29400 \pm 1200}{RT}\right)\right]_{A_2,\ 598\,K < T < 698\,K} \tag{7}$$

$$k^3_{D(NiO)} = \left[0.430 \times 10^9 \exp\left(-\frac{29400 \pm 2000}{RT}\right)\right]_{A_3,\ 598\,K < T < 698\,K} \tag{8}$$

$$k^{1a}_{D(NiO)} = \left[0.0196 \exp\left(-\frac{1000 \pm 280}{RT}\right)\right]_{A_1,\ 473\,K < T < 573\,K} \tag{9}$$

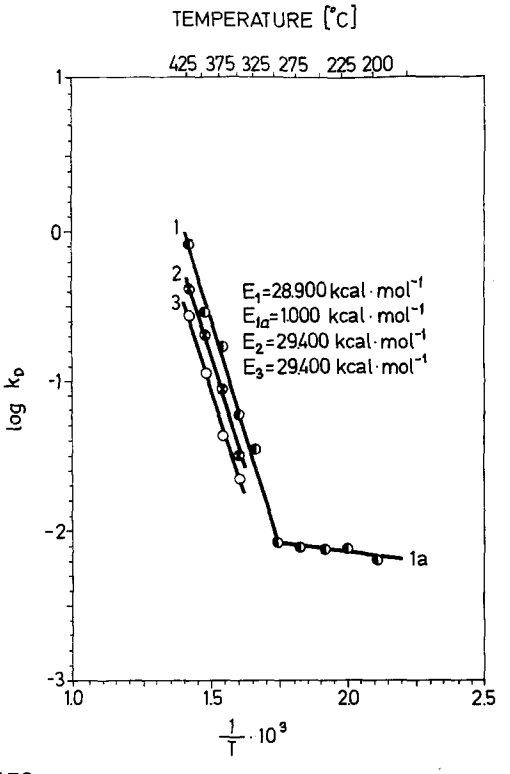

Figure 5 Log rate constant k_D versus $1/T$ for undoped NiO and the following oxygen doses: (1) and (1a) A_1, (2) A_2, (3) A_3.

with standard deviations:

$$\log k^1_{D(NiO)} = 0.0368 \tag{6a}$$

$$\log k^2_{D(NiO)} = 0.0172 \tag{7a}$$

$$\log k^3_{D(NiO)} = 0.0281 \tag{8a}$$

$$\log k^{1a}_{D(NiO)} = 0.0078. \tag{9a}$$

The fractions of oxygen consumed by the undoped NiO samples versus the times of the experiment described above and illustrated in Fig. 4, are plotted in Fig. 6. Comparing the curves in Figs. 4 and 6, one can observe that the maxima of the work function changes correspond to about 90% oxygen consumption by the sample and that shortly after reaching the maximum practically the whole oxygen dose is consumed. Applying the

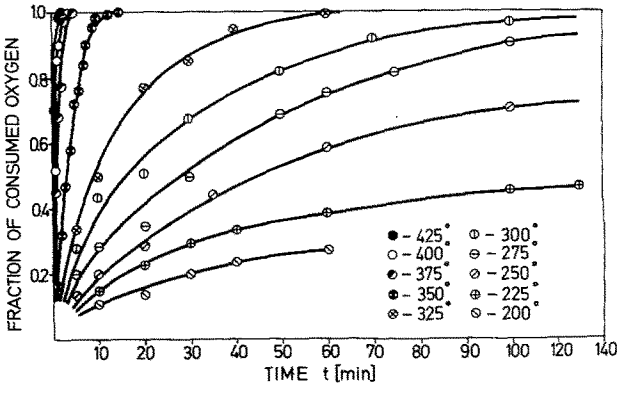

Figure 6 Fraction of consumed oxygen $q_{(t)}$ for undoped NiO versus time for the smallest oxygen dose, A_1.

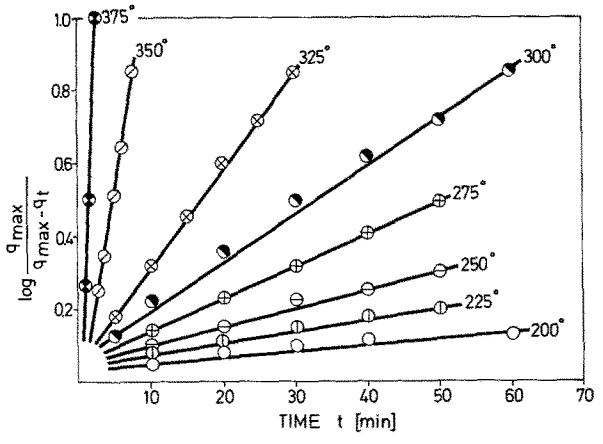

Figure 7 Plots of log $(q_{max}/q_{max} - q_{(t)}$ versus time.

same exponential relationship for the isothermal oxygen consumption versus time as that used for charging and discharging the surface:

$$q(t) = \{q_{max}[1 - \exp(-k_A t)]\}_{T=const.} \quad (10)$$

where $q(t)$ is the fraction of oxygen consumed in time t, q_{max} the maximal amount of the consumed oxygen, and k_A the rate constant of the sorption process, straight lines can be plotted in terms of the following co-ordinates (Fig. 7):

$$\ln \frac{q_{max}}{q_{max} - q(t)} = k_A t. \quad (11)$$

The rate constant of the process under consideration may thus be expressed:

$$k_A = \left[d \ln \frac{q_{max}}{q_{max} - q(t)} \right] \Big/ dt.$$

The dependence of the rate constant k_A on temperature fits the Arrhenius-type relationship (Fig. 8) well, showing the change in the activation energy at 300° C, similarly to that observed for the rate constant k_D versus $1/T$ (Fig. 5).

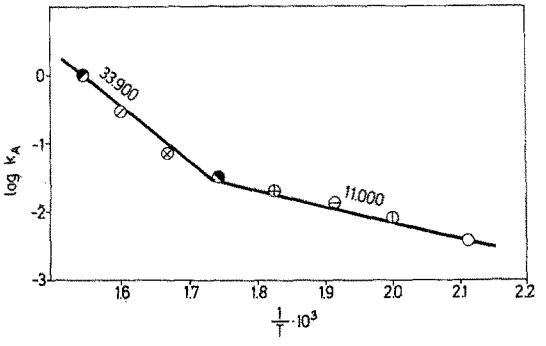

Figure 8 Rate constant k_A versus $1/T$.

4.2. Lithium-doped NiO

The changes in work function with time for lithium-doped NiO were measured for the smallest oxygen dose, A_1 (Table III), over the temperature range 300 to 400° C. As seen in Fig. 9, the work function first rapidly increases, then decreases and finally achieves the value $\Delta\Phi_S$ below the initial value. This effect (not reported for undoped samples) becomes less pronounced at higher temperatures and decreases from 0.035 eV at 300° C to 0.005 eV at 400° C (Fig. 9b). This work function changes were accompanied by a rapid de-

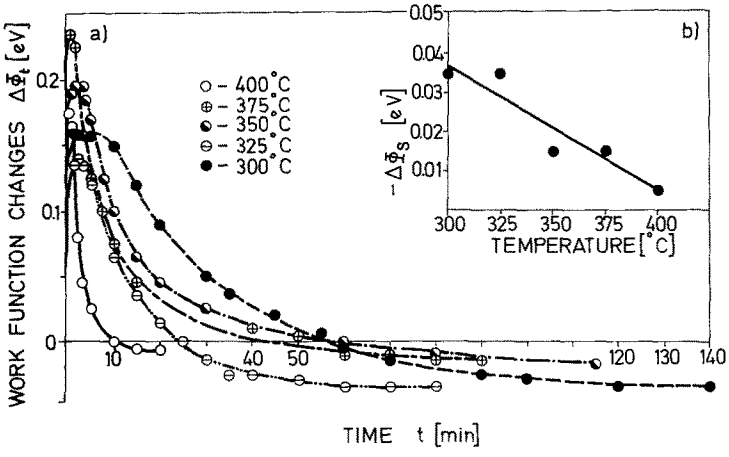

Figure 9 (a) Work function changes $\Delta\Phi$ for lithium-doped NiO versus time in the temperature range 300 to 400° C. (b) $\Delta\Phi_S$ plotted versus temperature.

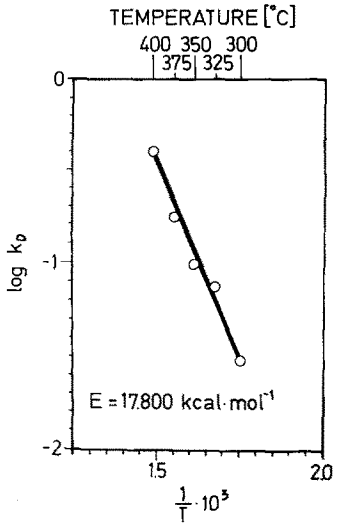

Figure 10 Log k_D plotted versus $1/T$ for lithium-doped NiO.

crease of oxygen pressure over the sample, similar to that observed for undoped NiO.

A straight line was fitted to the log k_D versus the reciprocal of the absolute temperature, $1/T$ plot, showing an activation energy of 17.8 ± 1.7 kcal mol^{-1} (Fig. 10). A least squares analysis yields the following expression for k_D versus temperature:

$$k_{D(NiO-Li_2O)} = \left[2.08 \times 10^5 \exp\left(-\frac{17\,800 \pm 1700}{RT}\right)\right]_{A_1,\ 573\,K < T < 673\,K} \quad (12)$$

with a standard deviation:

$$\log k_{D(NiO-Li_2O)} = 0.0339. \quad (12a)$$

4.3. CoO and Co_3O_4

The amounts of oxygen in the experimental dose required to achieve a pronounced effect on $\Delta\Phi(t)$ for both CoO and Co_3O_4 were considerably larger than that for NiO samples (A_5 in Table III). Plots of the work function changes versus time for CoO and Co_3O_4 were similar to those for NiO. A rapid consumption of oxygen from the gas phase was observed.

The calculated values of k_D fit the Arrhenius-type relationship (Fig. 11) well, yielding the following expressions:

$$k_{D(CoO)} = \left[1.984 \times 10^6 \exp\left(-\frac{18\,300 \pm 1000}{RT}\right)\right]_{A_5,\ 498\,K < T < 623\,K} \quad (13)$$

$$k_{D(Co_3O_4)} = \left[7.71 \times 10^6 \exp\left(-\frac{19\,900 \pm 3100}{RT}\right)\right]_{A_5,\ 498\,K < T < 623\,K} \quad (14)$$

with standard deviations:

$$\log k_{D(CoO)} = 0.0447 \quad (13a)$$

$$\log k_{D(Co_3O_4)} = 0.0987 \quad (14a)$$

4.4. Discussion of errors

The absolute values of the standard deviations of k_I, k_D, $\Delta\Phi_{max}$ and $\Delta\Phi_S$ cannot be calculated easily because the kinetic equation (Equation 5)

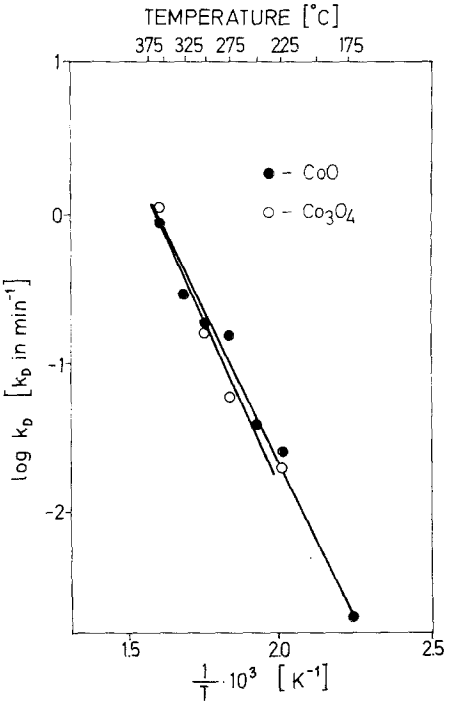

Figure 11 Log k_D versus $1/T$ for CoO and Co_3O_4.

does not have an analytical solution. Let $\Delta\Phi(t)$ be the solution of Equation 5 satisfying the intial condition (Equation 4) for the given parameters $\overline{k_I}$, $\overline{k_D}$, $\overline{\Delta\Phi_{max}}$ and $\overline{\Delta\Phi_S}$. For a given experimental function $\Delta\Phi(t)$, one should determine the values of k_I, k_D, $\Delta\Phi_{max}$ and $\Delta\Phi_S$ which should satisfy the following inequality for all possible values of $\overline{k_I}$, $\overline{k_D}$, $\overline{\Delta\Phi_{max}}$ and $\overline{\Delta\Phi_S}$:

$$(k_I, k_D, \Delta\Phi_{max}, \Delta\Phi_S) \leqslant (\overline{k_I}, \overline{k_D}, \overline{\Delta\Phi_{max}}, \overline{\Delta\Phi_S}) \quad (15)$$

where:

$$\epsilon(\overline{k_I}, \overline{k_D}, \overline{\Delta\Phi_{max}}, \overline{\Delta\Phi_S}) = \sum_{i=1}^{n} [\Delta\Phi(t) - \Delta\Phi(t)]^2. \quad (16)$$

A least-squares analysis cannot be applied here since $\Delta\Phi(t)$ is not a linear function of k_I, k_D, $\Delta\Phi_{max}$ and $\Delta\Phi_S$. The minimum of the Equation 16 may, therefore, be determined using the inconvenient iterative method. The correctness of the calculations was verified by the standard deviation between the experimentally measured values of the work function changes $-\Delta\Phi(t)$ and those calculated $-\Delta\Phi(t)_{calc}$:

$$\text{S. D.} = \left\{ \sum_{i=1}^{n} [\Delta\Phi(t) - \Delta\Phi(t)_{calc}]^2/n - 1 \right\}^{1/2}. \quad (17)$$

This standard deviation was found to be approximately 0.02 eV for both NiO and NiO–Li_2O and 0.015 eV for both CoO and Co_3O_4, which is always lower than 10% of the maximum value of $\Delta\Phi(t)$. Numerical analysis of the kinetic equation (Equation 5) has shown that the average deviation of k_I, k_D, and $\Delta\Phi_{max}$ does not surpass: 75%, 20% and 15%, respectively [41]. $\Delta\Phi_S$ may be determined experimentally within an accuracy of about 0.01 eV, and the temperature was measured to within of ± 2° C.

The $\Delta\Phi(t)$ results for NiO are easily reproducible both for several successive measurements on the same sample, if the oxygen dose is sufficiently small, and for three independent measurements on three different samples of the same preparation, if the standarization procedure is carefully repeated. Fig. 12 shows the reproducibility of the measured values of $\Delta\Phi(t)$ for undoped NiO at 400° C and for the smallest oxygen dose, A_1, taken from three successive readings. However, if between each measurement the oxide sample is subjected to adsorption and desorption of oxygen under a pressure of several mm Hg, then the work function data only become reproducible after several adsorption–desorption operations. Fig. 13a shows four experimental runs for NiO at 400° C and oxygen dose A_1 where each run of $\Delta\Phi(t)$ was preceded by adsorption of oxygen under 10 mm Hg and followed by desorption under 10^{-6} mm Hg. Fig. 13b shows the kinetics of sorption of

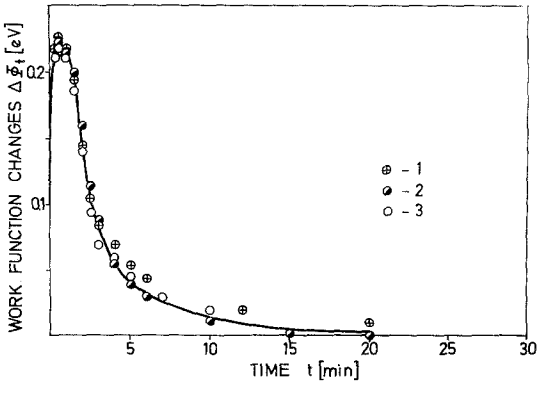

Figure 12 The reproducibility of three consecutive experimental runs $\Delta\Phi$ versus time at 400° C for undoped NiO.

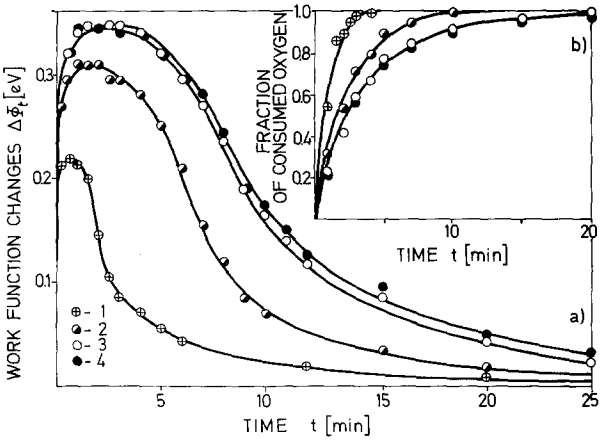

Figure 13 The reproducibility of four experimental runs at 400° C – (a) $\Delta\Phi$ versus time and (b) fraction of oxygen consumption versus time – taken after consecutive standardization of the NiO sample in oxygen under 10 mm Hg.

oxygen accompanying the work function changes in Fig. 13a. These experiments illustrate that the oxide sample acquires its reproducible properties during the course of several runs. These data characterize the problem of the reproducibility of any surface parameter of metal oxide measured below the temperature corresponding to the equilibrium between gaseous oxygen and the crystalline bulk. The results in Fig. 13 indicate that good reproducibility of the oxide surface properties requires the oxide sample to be carefully and suitable standardized.

The reproducibility of the work function data $\Delta\Phi(t)$ for both CoO and Co_3O_4 requires investigation using different samples.

5. Discussion

5.1. Re-equilibration mechanism

After the oxygen dose is adsorbed on the standardised oxide surface, the chemical potential of both ions and electronic carriers tends to reach a new equilibrium state. This re-equilibration thus involves the flow of both metal ions and electrons exhibiting an opposite effect. A more rapid electronic process involves fast ionization of the adsorbed oxygen species and formation of the surface space charge layer enriched in electron holes. This process may also be considered as equivalent to the generation of cation vacancies on the oxide surface creating a "source" of non-stoichiometry corresponding to the experimental oxygen dose. Thus the initial rapid increase in work function corresponds to the formation of negatively charged oxygen species such as O_2^-, O_2^{2-}. O^- and finally as O^{2-}, being generally considered stable only if incorporated into the oxide lattice and stabilized in the cyrstal field. The latter process may be expressed for NiO, as an example, by the reaction*:

$$\tfrac{1}{2}O_{2(ads)} \rightleftharpoons O_O^x + V_{Ni}$$

The generated cation vacancies are generally considered to act as acceptor centres which may be singly or doubly ionized:

$$V_{Ni} \rightleftharpoons V'_{Ni} + h\cdot$$

$$V'_{Ni} \rightleftharpoons V''_{Ni} + h\cdot$$

where V_{Ni}, V'_{Ni}, V''_{Ni} are neutral, single doubly ionized cation vacancies, O_O^x is the oxygen in the lattice position, and $h\cdot$ an electron hole.

According to Osburn and Vest [42] both singly and doubly ionized forms can appear in the crystalline bulk of NiO over temperature range used (300 to 400° C). Graham and Cohen [43] have found that the parabolic rate constant depends on the oxygen pressure at 400° C by the power $\frac{1}{6}$, which suggests the presence of doubly ionized cation vacancies in NiO [37].

The diffusion of the cation vacancies in towards the bulk causes discharging of the surface, thus producing a decrease in work function. This diffusion process occurring under a concentration gradient (termed chemical diffusion) is assumed to be the rate controlling process for the observed decrease in work function after passing through a maximum. Such a diffusion of cation vacancies from the surface towards the bulk (this process may also be considered as the transport of cations from the bulk towards the surface) is accompanied by the diffusion of electron carriers

*The Kroger–Vink notation is used.

(ambipolar diffusion) obeying the electroneutrality condition:

$$[V'_{Ni}] + 2[V''_{Ni}] = [h^{\bullet}]$$

where the brackets denote the concentration. The electrostatic field which arises in the oxide boundary layer as a result of oxygen chemisorption accelerates the transport of cation vacancies from the surface in towards the bulk. Owing to the difference in the rate constants of both charging and discharging processes (related to electronic and ionic processes, respectively) the measured work function changes with time exhibit a pronounced maxima as seen in Fig. 2, 4, 9, 11 and 12.

5.2. Discussion of the kinetic equation parameters

Fig. 2b, c and d show the parameters k_I, k_D and $\Delta\Phi_{max}$ of the kinetic equation (Equation 5) plotted versus the amount of oxygen in the experimental dose for undoped NiO. As seen, both k_I and k_D decrease with the increasing amount of oxygen, whereas $\Delta\Phi_{max}$ increases.

It appears that the observed trend of k_I changes is caused by energetic inhomogenity of the oxide surface involving non-uniform activity of the adsorbing centres. Accordingly, the first oxygen atoms occupy the most energetically convenient centres, whereas later atoms are bound by successively less and less active centres.

Assuming the rate constant of discharging to be rate controlled by the chemical diffusion, we can relate k_D to the chemical diffusion coefficient. Such a diffusion coefficient should be independent of the defect concentration at the small concentrations as expected theoretically, and found experimentally for both NiO and CoO [4, 44, 45]. At larger concentrations of defects, e.g. for the wustite phase, the chemical diffusion coefficient is inversely proportional to the concentration and this effect is believed to be produced by interaction between defects [3, 4]. Therefore the observed dependence of the rate constant k_D on the amount of oxygen in the experimental oxygen dose (Fig. 2c) seems to indicate an interaction between the cation vacancies generated at the NiO surface in spite of the fact that the bulk NiO grains exhibit a very small deviation from stoichiometry amounting to about 0.01 at.% under equilibrium conditions (1000° C, p_{O_2} = 1 atm). However, the initial surface concentration of the cation vacancies generated in strong electric field of the boundary layer is expected to be of the same order of magnitude as the concentration of the adsorbed oxygen species to be incorporated (Table III). At this concentration (several at.%) cation vacancies may interact, and thus the chemical diffusivity of the boundary layer may show a dependence on defect concentration. This interaction seems to be responsible for the observed dependence of the rate constant k_D on the amount of oxygen in the dose (Fig. 2c).

As seen from Fig. 3b and c, the value of k_D is approximately one order of magnitude smaller than that of k_I. This illustrates well the difference between the rate of the electronic and ionic equilibration processes.

The relation between $\Delta\Phi_{max}$ and the amount of oxygen in the dose (Fig. 2d) is in good agreement with the conclusions of the electronic theory of chemisorption on semiconductors [13, 14].

The final value of the work function change with respect to the initial value can be ascribed to the change in the structural surface properties during the experiment. Hence we might expect that the re-equilibration process involving the generation and propagation of cation vacancies should lead to a certain final electronic effect represented by the parameter $\Delta\Phi_S$ in Equation 5. In fact, this effect for undoped samples is not measurable and thus does not exceed the value of the experimental accuracy 0.01 eV, except in the case of larger oxygen doses (curves A_3 and A_4 in Fig. 2a).

It is surprising that despite formation of acceptor centres accompanying the incorporation of oxygen into the lattice of lithium-doped NiO, the sign of $\Delta\Phi_S$ is negative, thus indicating an increase in the final Fermi level (Fig. 9b). The observed effect may be caused by the participation of the lithium ions in the diffusion through the boundary layer. Its prevailing influence in the observed effect seems to consist in changing the defect structure of the new lattice elements formed on the surface of the NiO crystal. Generally, it is obvious that this effect should be attributed either (1) to an enrichment of the surface layer in the donor centres, or (2) to an impoverishment in the acceptors.

(1) Cations localized interstitially as well as anion vacancies may be considered as donors being formed according to the equilibria:

$$Li_2O + 2h^{\cdot} \rightleftharpoons 2Li_i^{\cdot} + \tfrac{1}{2}O_2 \qquad (a)$$

$$Li_2O \rightleftharpoons 2Li'_{(Ni)} + V_O^{\cdot\cdot} + O_2 \qquad (b)$$

where Li_i and $Li_{(Ni)}$ denote lithium in the interstitial and lattice positions, respectively, and V_O is the anion vacancy. According to the thermodynamic treatment of Fischer and Wagner [46] the concentration of interstitial cations increases with decreasing oxygen pressure over lithium-doped NiO. Thus the low experimental oxygen partial pressure favours equilibrium a to be shifted to the right. The same mechanism of lithium incorporation was also discussed by Bielański *et al.* as being possible in the surface layer of lithium-doped NiO catalysts [6, 7, 38].

Many experiments concerning, for example, oxygen desorption data [47] or isotopic exchange [48], indicate that anion vacancies may also be formed in the oxide surface layer as a result of lithium incorporation into NiO. Recently, Degraix and co-workers [49, 50], in studying several properties of $NiO-Li_2O$ solid solutions, have postulated that the incorporation of lithium ions into the NiO lattice creates and stabilizes anion vacancies according to reaction b.

(2) The decrease in the concentration of acceptor centres in the surface layer may be considered as caused by evaporation of lithium located in the cation sublattice of NiO:

$$Li_2O \rightleftharpoons 2Li'_{(Ni)} + 2h^{\cdot} + \tfrac{1}{2}O_2. \qquad (c)$$

It is difficult to decide which of the above processes is responsible for the observed electronic effect, although mechanisms a and b seem to be preferable for the surface layer. However, this effect supports the previous suggestion concerning the divergence in structural properties between the bulk and the surface layer.

In the case of both CoO and Co_3O_4 preparations, the same dependence was observed for the parameters of Equation 5 against the oxygen dose, as for NiO. The amount of oxygen consumed by both the CoO and Co_3O_4 samples (dose A_5 in Table III) is markedly higher than that sorbed (for corresponding times) by both undoped and lithium-doped NiO. This effect remains in good agreement with the fact that the defect concentration of NiO is markedly lower than that of CoO [2, 37]. The kinetic data obtained (Equations 15 and 16) also indicate that the diffusivity of the surface layer of Co_3O_4 is similar to that of CoO, assuming both are standardized in the same way.

5.3. Equilibration kinetics

The high activation energy of the discharge of the NiO surface above 300° C (28.9 kcal mol) suggests that this process is rate controlled by the lattice ionic diffusion. It is interesting to compare this determined value of the activation energy with that determined previously at higher temperatures using the electrical conductivity technique for monitoring the re-equilibration kinetics in the crystalline bulk of NiO. Wagner and co-workers reported values of 21.9 kcal mol^{-1} [1] and 21.7 kcal mol^{-1} [51], whereas Mrowec and co-workers gave a value of 33.7 kcal mol^{-1} [52]. The activation energy given here and which is believed to characterize the chemical diffusivity in the surface layer, is therefore higher than that reported by Wagner and co-workers [1, 51] but lower than that given by Mrowec and co-workers [52]. It is also seen from Fig. 6 that the activation energy determined here is practically independent of the amount of oxygen in the dose.

The considerably smaller activation energy below 300° C (1 kcal mol^{-1}) suggests that in this case, the surface potential changes are caused by a different mechanism leading to discharging of the surface. This mechanism may involve the surface diffusion of the adsorbed oxygen species within the adsorbed layer from statistical adsorption sites to the sites energetically more convenient.

The kinetic data of the sorption of oxygen on the NiO surface also show a break at 300° C, with 33.9 kcal mol^{-1} above and 11.0 kcal mol^{-1} below this temperature (Fig. 8b). This fact supports the above postulation concerning the changes of the character of the oxygen interaction with the NiO surface near this temperature. The higher activation energy value determined above 300° C confirms that the sorption process is rate controlled by the lattice chemical diffusion. The lower activation energy below 300° C corresponds to chemisorption of oxygen on NiO surface.

These considerations indicate that above 300° C the NiO lattice becomes sufficiently mobile to enable ionic diffusion through the surface layer to take place. Using available chemical diffusion data extrapolated to the temperature range of the present investigations, one may calculate that in the experimental conditions described in this work the depth of diffusion penetration for NiO at 350° C and for 1 h, amounts to 10^{-4} cm below the surface of the crystal grain. Thus we may expect that changes in oxygen partial pressure over the

NiO crystal will lead to changes in the defect structure of such a surface layer.

The question concerning the changes in the mechanism of discharging the surface at 300° C seems to be connected with the explaination of the transition of the non-equilibrium to the equilibrium branch of the oxygen adsorption isobar for NiO. This transition takes place near 300° C [40, 53, 55]. As generally postulated, the chemisorption equilibrium is reached very quickly above 300° C, whereas below this temperature is not attained. However, taking into account the present results one may suppose that the process of interaction between gaseous oxygen and the NiO surface is more complex, also involving changes in the defect structure of the surface layer. Thus, in this case a quasi-equilibrium between gas phase and a layer near to the surface, should also be considered above 300° C, although the crystalline bulk is situated far away from the thermodynamic equilibrium. On the other hand, ionic transport through the NiO lattice slows down considerably below 300° C, thus leading to a retardation of linked adsorption equilibria.

The changes in the kinetics of oxygen adsorption as well as in many other surface properties have also been reported for NiO in the temperature range 250 to 300° C [56–69]. Mekhandjiev and Bliznakov have found a sharp increase in the activation energy for CO oxidation at 250° C with NiO as a catalyst [60, 61]. Winter and Co-workers [62. 63] has interpretated the change of oxygen isotopic exchange and oxygen adsorption data of NiO at 250° C as being caused by the formation and destruction of the magnetic domains accompanying stress and relaxation of the lattice at the Néel temperature which was found to be 250° C for undoped NiO [64]. The Néel temperature of NiO decreases sharply with lithium addition up to about 170° C for 9 at. % Li_2O [64]. The change of the effect of an electric field on nickel oxidation near the Néel temperature has been reported by Ritchie *et al.* [65].

The present conclusions on the increasing mobility of the cation sublattice in NiO above the transition temperature of about 250 to 300° C is supported by the results of investigations on the formation of NiO–Li_2O solid solutions. According to the works of Iida *et al.* [66], Tseung and Bevan [67] and Degraix and co-workers [49, 50], the lithium ions may already be incorporated into the NiO lattice at 250° C.

The reproducibility of the work function changes accompanying oxygen adsorption and desorption was also observed above 300° C for both single- and polycrystalline NiO [68, 69]. The temperatures corresponding to the change in several properties of NiO are illustrated in Table V. The slight differences in the values of temperature reported by different authors may be ascribed to different standardization procedures having an effect on the initial properties of the NiO preparations as well as to the level of impurities.

The kinetic data for discharging the surface of lithium-doped NiO in the temperature range 300 to 400° C lead to an activation energy of 17.8 kcal mol^{-1} (Fig. 9), which is lower than that for the undoped sample. This comparison would point to interstitial mechanism a which may produce a lattice expansion leading to a lowering of the activation energy of the diffusion process. Unfortunately, there is a lack of diffusion data referring to the NiO–Li_2O system, thus this problem remains open to further investigation and discussion.

The activation energies for discharging the surface of CoO and Co_3O_4 amount to 18.3 and 19.9 kcal mol^{-1}, respectively. This indicates that independent of the initial structure of CoO and Co_3O_4, the experimental procedure described above favours the formation of surface layers characterized by the same activation energy of chemical diffusion. The experimental temperature range, 175 to 350° C, is too low to bring the bulk of the crystalline grain into equilibrium with oxygen. The present results indicate, however, that this temperature range is high enough for the oxide surface layer (about 10^{-4} cm deep) to achieve quasi-equilibrium with the oxygen gas phase. The values of the activation energy obtained here are very close to the activation energy of chemical diffusion measured by Price and Wagner [1] (24 kcal mol^{-1}).

The discussion above is based on the assumption that the measured work function changes are determined by the changes of the potential drop in the space charge of the oxide boundary layer. As is usually assumed, the potential drop due to the dipole moment of the molecules adsorbed on a semiconductor is considerably smaller than that produced by the space charge [70]. Therefore, the dipole moment component of the work function changes can be neglected. Recently Tscherkhashin has claimed to have shown that these two com-

TABLE V Temperatures at which several properties of NiO change

No.	Temperature (°C)	Effect	References
1	250–300	Maximum on oxygen adsorption isobar	[40]
2	300	Maximum on oxygen adsorption isobar	[53]
3	300	Maximum on oxygen adsorption isobar	[54]
4	300	Maximum on oxygen adsorption isobars	[35]
5	200–300	Kinetics of oxygen adsorption	[56]
6	250	Kinetics of oxygen adsorption	[57]
7	250	Kinetics of oxygen adsorption	[58]
8	238–275	Heat of oxygen adsorption	[59]
9	250	Catalytic and magnetic properties	[60]
10	250	Adsorption, magnetic and catalytic properties	[61]
11	250	Kinetics of oxygen adsorption and isotopic exchange	[62]
12	250	Specific surface area determined after several runs of catalytic reaction	[63]
13	250	Magnetic susceptibility	[64]
14	350	Mechanism of Ni oxidation in the electric field	[65]
15	300	Formation of $NiO–Li_2O$ solid solution	[66]
16	below400	Formation of $NiO–Li_2O$ solid solution	[67]
17	250	Formation of $NiO–Li_2O$ solid solution	[49, 50]
18	300	Effect of oxygen adsorption on the character of the work function changes of polycrystalline NiO	[68]
19	300	Effect of oxygen adsorption on the character of the work function changes of single-crystal NiO	[69]
20	300	Mechanism of discharging the surface	Present results

ponents of the work function changes are of the same order of magnitude [71]. His conclusion is based on both optical and thermal work function measurements. However, both these techniques are subject to large experimental errors in the work function data. Moreover, his results (as yet not confirmed in any other laboratory) seem to be still open to discussion. It should be also emphasized that even if Tscherkhashin's estimation were correct it would not contradict the argument presented in this paper. The process of discharging the surface is evidently composed of not only the vanishing of space charge in the boundary layer of the adsorbent connected with outward cation diffusion, but also the incorporation of the adsorbed oxygen atoms into the surface of the NiO lattice, the latter being equivalent to the vanishing of surface dipoles, if any. However, the process of chemical diffusion through the oxide lattice should always remain the rate determining step of the discharging process.

6. Conclusions

The presented results and their discussion lead to several conclusions on more general aspects:

(1) Good agreement between the experimental data and the kinetic equation (Equation 5) indicate that the kinetic equation may be applied for quantitative interpretation of the transport processes in the boundary layer of ionic oxides.

(2) The presented research indicates that the defect structure of the layer near to the surface may be regulated by changing oxygen partial pressure in the region of 300° C for Nio and at 200° C (or below) for both CoO and Co_3O_4, although under these conditions, the crystalline bulk remains isolated from the thermodynamic equilibrium state.

(3) The thermodynamic equilibrium between metal oxide and gaseous oxygen may be considered to be composed of several partial quasi-equilibria (Fig. 14):

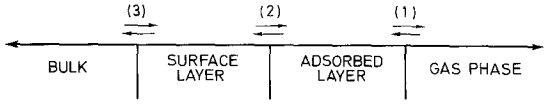

Figure 14 The hypothetical model for the metal oxide–oxygen system.

(a) chemisorption equilibrium between gaseous oxygen and chemisorbed oxygen on the oxide surface (equilibrium 1);

(b) equilibrium between chemisorbed oxygen and the oxide surface layer (equilibrium 2);

(c) equilibrium between the surface layer and the bulk (equilibrium 3).

The oxide–oxygen system may thus be considered initially as only equilibrium 1, whereas equilibria 2 and 3 are "quenched", then, as the temperature increases, as the sum of equilibria 1 and 2, and finally, at high temperatures, as the sum of all three equilibria. When considering the transport properties of metal oxides at high temperatures one may expect that all equilibria may be established very quickly. It is generally assumed that the rate of equilibration between gaseous oxygen and the oxide crystalline bulk is controlled by equilibrium 3. It seems, however, that the rate of such an equilibration may also be controlled by equilibrium 1 or 2, in so called "surface controlled" mechanisms. In these cases investigation of transport properties of the crystalline bulk requires that the properties of the oxide surface layer are treated independently.

The above conclusions seem to be important in adjusting the optimal conditions of the standardization of oxide catalysts and may also be useful in the interpretation of the mechanism of catalytic oxidation processes on metal oxides. Moreover, the proposed method of investigation of the re-equilibration kinetics of the oxide surface layer would appear to have a practical application in studying the transport processes in metal oxides.

Acknowledgements

The author is indebted to Professors A. Bielański and J. Haber for their remarks, and to Drs K. Dyrek and Z. Kluz, who kindly supplied the lithium-doped NiO preparation.

References

1. J. B. PRICE and J. B. WAGNER, Jun., *Z. Physik. Chem. N. F.* **49** (1966) 257.
2. J. B. WAGNER, Jun., "Mass Transport in Oxides", NBS Special Publication 296 (1968) 65.
3. P. E. CHILDS and J. B. WAGNER, Jun., "Heterogeneous Kinetics at Elevated Temperature" (Plenum Press, New York, 1970) p. 269.
4. P. E. CHILDS, L. W. LAUB and J. B. WAGNER Jr., *Proc. Brit. Ceram. Soc.* **19** (1971) 29.
5. A. V. KRILOVA, L. Ya. MARGOLIS and G. I. TSCHIZHIKOVA, *Kinetika i Kataliz* **6** (1965 854.
6. J. DEREŃ, J. NOWOTNY and J. ZIÓLKOWSKI, *Bull. Acad. Polon. Sci. Ser. Sci. Chim.* **16** (1968) 45.
7. A. BIELAŃSKI, J. DEREŃ, K. DYREK, R. DZIEMBAJ, J. NOWOTNY and E. WENDA, *ibid* **18** (1970) 357.
8. I. S. SAZONOVA, N. P. KEIER, T. P. KHOKHLOVA and I. L. MIKHAILOVA, *Kinetika i Kataliz* **11** (1970) 447.
9. F. L. WILLIAM and D. NASON, *Surface Sci.* **45** (1974) 377.
10. C. LEYGRAF, G. HULTQUIST and S. EKELUND, *ibid* **46** (1974) 157.
11. J. DEREŃ, B. RUSSER, J. NOWOTNY, G. RÓG and J. SŁOCZYŃSKI, *J. Catalysis* **34** (1974) 124.
12. N. B. HANNAY, Ed. "Semiconductors" (Reinhold, New York, and Chapman and Hall, London, 1959).
13. F. F. VOLKENSTEIN, "Electronic theory of chemisorption and catalysis on semiconductors" (Pergamon Press, New York, 1964).
14. K. HAUFFE, "Reaktionen in und an Festen Stoffen" (Springer Verlag, Berlin 1966).
15. A. A. HOLSCHER, *Surface Sci.* **4** (1966) 89.
16. T. DELCHAR, F. C. TOMPKINS, *ibid* **8** (1967) 165.
17. J. C. RIVIERE, "Work Function Measurements and Results", Rep. U.K. Atomic Energy Authority, Metall. Div., Harwell, Oxon (1967).
18. D. NENOW, *Surface Sci.* **8** (1967) 453.
19. E. E. HUBER Jr. and C. T. KIRK Jr., *ibid* **8** (1967) 458.
20. *Idem, ibid* **9** (1968) 217.
21. M. W. ROBERTS, "Recent Progress in Surface Science", Vol. 3 (Academic Press, 1970) p.1.
22. R. DUŚ, *Trans. Faraday Soc.* **69** (1973) 878.
23. M. W. ROBERTS and B. R. WELLS, *ibid* **62** (1966) 1608.
24. *Idem, Surface Sci.* **8** (1967) 453.
25. N. A. SHURMOVSKAYA and R. C. BURSHTEIN, *ibid* **2** (1964) 210.
26. J. NOWOTNY, *Bull. Acad. Polon. Sci. Sér. Sci. Chim.* **21** (1973) 413.
27. V. I. LIASHENKO and I. I. STIEPKO, *Izv. Akad. Nauk SSSR Ser. Fiz.* **21** (1957) 201.
28. E. Kh. ENIKEEV, O. V. ISAIEV and L. Ya. MARGOLIS, *Kinetika i Kataliz* **1** (1960) 431.
29. I. SCHEVE and A. V. KRILOVA, *ibid* **11** (1970) 259.
30. S. BOURASSEAU, Thése no. 189, l'Universite Claude Bernard, Lyon (1973).
31. J. NOWOTNY and M. DESTRIAU, *Bull. Soc. Chim. France* (1976), 91.
32. J. NOWOTNY, *Bull. Acad. Polon. Sci. Sér. Sci. Chim.* **17** (1969) 173.
33. J. DEREŃ and J. NOWOTNY, *Oxid. Metals* **1** (1969) 73.
34. A. J. BOSMAN and C. CREVECOEUR, *Phys. Rev.* **144** (1966) 763.
35. S. PIZZINI, W. MONARI and R. MORLOTTI, *J. Electrochem. Soc.* **118** (1971) 796.
36. J. DEREŃ and M. RĘKAS, *Roczn. Chem.* **46** (1972) 1411.

37. P. KOFSTAD, "High temperature oxidation of metals" (John Wiley, New York, 1966).
38. A. BIELAŃSKI, K. DYREK, Z.KLUZ, J. SLOCZYŃSKI and T. TOBIASZ, *Bull. Acad. Polon. Sci. Sér. Sci. Chim.* **12** (1964) 657.
39. R. CHRUŚCIEL, J. DEREŃ and J. NOWOTNY, *Exp. Tech. Phys.* **14** (1966) 127.
40. J. HABER and F. S. STONE, *Trans. Farad. Soc.* **59** (1963) 192.
41. S. BIALAS and J. NOWOTNY, *Bull. Acad. Polon. Sci. Sér. Sci. Chim.* **21** (1973) 923.
42. C. M. OSBURN and R. W. VEST, *J. Phys. Chem. Solids* **32** (1971) 1343.
43. M. J. GRAHAM and M. COHEN, *J. Electrochem Soc.* **119** (1972) 879.
44. S. MROWEC, *J. Mater. Sci.* **9** (1974) 1961.
45. E. FRYT, S. MROWEC and T. WALEC, *Oxid. Metals* **7** (1973) 117.
46. B. FISCHER and J. B. WAGNER Jr., *Phys. Letters* **21** (1966) 606.
47. A. BIELAŃSKI, J. DEREŃ, J. HABER and J. SLOCZYŃSKI, *Trans. Farad. Soc.* **58** (1962) 166.
48. N. P. KEIER, *Kinetika i Kataliz* **1** (1960) 221.
49. H. DEGRAIX, Thése no. 56, l'Universitè Claude Bernard, Lyon (1971).
50. H. DEGRAIX, P. C. GRAVELLE and S. J. TEICHNER, *J. Solid. State Chem.*
51. J. NOWOTNY and J. B. WAGNER, *Jun., J. Amer. Ceram. Soc.* **56** (1973) 397.
52. J. DEREŃ, Z. M. JARZĘBSKI, S. MROWEC and T. WALEC, *Bull. Acad. Polon. Sci. Sér. Sci. Chim.* **19** (1971) 153.
53. J. DEREŃ and J. STOCH, *J. Catal.* **18** (1970) 249.
54. A. KOWALSKA and R. GAJERSKI, *Zeszyty Naukowe AGH, Ceramika* **18** (1974) 19.
55. J. DEREŃ and A. KOWALSKA, *ibid* **18** (1974) 7.
56. H. J. ENGELL and K. HAUFFE, *Z. Elektrochem.* **57** (1953) 762, 773.
57. L. N. KUTSEVA and N. P. KEIER, *Problemy Kinetyki i Kataliza Akad. Nauk SSSR* **10** (1960) 82.
58. H. B. CHARMAN, R. M. DELL and S. S. TEALE, *Trans. Farad. Soc.* **59** (1963) 453.
59. YU. D. PANKRATIEV, N. P. KEIER, V. I. SOBOLEV and G. Y. GRIDASOVA, *Kinetika i Kataliz* **11** (1970) 1279.
60. D. MEKHANDJIEV and G. BLIZNAKOV, *Compt. Rend. Acad. Bulg. Sci.* **19** (1966) 45.
61. D. MEKHANDJIEV, Ph. D. Thesis., Institute of General and Inorganic Chemistry, Bulg. Acad. Sci., Sofia (1968).
62. E. R. S. WINTER, *J. Catalysis* **6** (1966) 35.
63. L. D. EATON and E. R. S. WINTER, *ibid* **4** (1965) 552.
64. R. M. NOTIS, R. M. SPRIGGS and W. C. HAHN Jr., *J. Appl. Phys.* **44** (1973) 4165.
65. I. M. RITCHIE, G. H. SCOTT and P. J. FENSHAM, *Surface Sci.* **19** (1970) 230.
66. YOSHIO IIDA, SHURNO OZAKI and Kenzo SHIMADA, *Bull. Chem. Soc. Jap.* **33** (1960) 656.
67. A. C. C. TSEUNG and H. L. BEVAN, *J. Mater. Sci.* **5** (1970) 604.
68. J. DEREŃ, J. NOWOTNY and J. ZIÓLKOWSKI, *Bull. Acad. Polon. Sci. Sér. Sci. Chim.* **15** (1967) 109.
69. J. DEREŃ, J. NOWOTNY and A. SADOWSKI, *ibid* **21** (1973) 503.
70. S. Z. ROGIŃSKI, *Kinetika i Kataliz* **1** (1960) 15.
71. A. E. TSCHERKHASHIN, Ph. D. Thesis, Institute of Catalysis, Sibirian Branch of the Academy of Sciences of USSR, Novosibirsk (1971).

Received 9 March and accepted 27 August 1976.